

We are IntechOpen, the world's leading publisher of Open Access books Built by scientists, for scientists

6,900

Open access books available

186,000

International authors and editors

200M

Downloads

Our authors are among the

154

Countries delivered to

TOP 1%

most cited scientists

12.2%

Contributors from top 500 universities



WEB OF SCIENCE™

Selection of our books indexed in the Book Citation Index
in Web of Science™ Core Collection (BKCI)

Interested in publishing with us?
Contact book.department@intechopen.com

Numbers displayed above are based on latest data collected.
For more information visit www.intechopen.com



Fluorescent Nanoagents for Biomedical Applications

*Dmitry Korolev, Maria Istomina, Anton Belorus,
Artem Brovko, Dmitry Sonin, Galina Shulmeyer,
Natalya Evreinova and Vyacheslav Moshnikov*

Abstract

Fluorescence imaging is a promising method widely used for the evaluation of the biodistribution and accumulation of various fluorescent agents cross-linked to the drug for effective therapy control. This work presents the methods for the functionalization of nanomaterials to provide them with fluorescent properties. The first of these methods is a unique technology for producing porous silicon with fluorescent properties. The second approach demonstrates linking of the fluorophores to inorganic nanoparticles (NP) using a spacer molecule ending with a functional group. For all these examples of fluorophores, biodistribution studies were performed with the fluorescent imaging system IVIS Lumina LT III (PerkinElmer, USA). It was noted that the size of particles and the method of their injection affect the distribution and accumulation in organs. The resulting materials can be used to develop platforms for theranostics.

Keywords: fluorescence, imaging, biodistribution, nanoagents, fluorophores, nanomaterials, theranostics

1. Introduction

Fluorescent imaging is nowadays being widely developed in biology, experimental and practical medicine, and both on cells in vitro and on living organisms in vivo [1]. The main advantages of this method are an increased contrast and the usage of several fluorescent agents working at different wavelengths. Among the other features of the method are low concentrations of agents, simplicity, and relative cheapness of the hardware design.

It happens, often, that the area of localization and distribution of the studied substances after injection is unknown. The application of the fluorescence imaging in preclinical studies allows us to noninvasively track the total biodistribution, localization, and accumulation of the injectable drugs with a fluorescent label complementary to the studied structures [2–7].

Fluorescence tomography has been used in practical medicine for about 50 years. Currently, there are only two fluorescent agents in the world, indocyanine green (ICG) and fluorescein (FLN), as well as their various chemical modifications, that are allowed for clinical use in vivo [8]. Fluorophores such as rhodamines B, 6G, 110, and 123 and thioflavins T and S are widely used in in vitro experiments.

Fluorescein and indocyanine green are primarily used for retinal angiogram investigations, which require an incomparably high dose of the agent. Herewith, the toxic effects of these fluorophores are not observed in vivo [9]. For molecular imaging, a reduced concentration of the fluorescent agent, which has minimal toxicity, is usually used [8].

Recently, active and activated complex fluorescent agents have been employed [10]. Active agents consist of fluorescent dyes conjugated with nanoobjects, enzymes, monoclonal antibodies, etc. Also, the liposomal forms of agents are used [11]. Activated agents contain a fluorophore in their composition, the fluorescence of which is suppressed during the storage and manipulation. The fluorescence radiation is obtained by chemical suppression of the quenching factor [12]. An example of this effect is the dimerization of ICG. In this case, it is possible to destroy dimers that are not capable of fluorescence by interacting with the blood protein—albumin [13].

ICG-labeled monoclonal antibodies to tumor cells allow the visualization of tumors, both in experimental (in vivo and ex vivo tomography) and in clinical practices during surgical interventions [14]. Optical tomography with implemented green indocyanine enables to identify the sentinel lymph nodes and preserving regional lymph nodes without metastases when removing a malignant tumor [15]. Liposomal ICG can be used for the evaluation of the drainage function of the lymphatic system and detect the spread of metastases by lymph drainage [16]. Physical adsorption of ICG and monoclonal antibodies on the free surface of liposomes is possible [17]. In this case, there is an increased quantum yield compared to the free, i.e., unbound ICG. Liposomes with incorporated polyethylene glycol (PEG) conjugate with ICG can be used for photoacoustic tomography [18]. In [19], the authors found that green indocyanine could be embedded in the membrane wall of lipids of liposomes. Herewith, it is possible to store such a drug at a temperature of +4°C for a fairly long period (more than 1 year).

The simplest and well-established nanoscale carriers of fluorophores are silica nanoparticles (NPS) and magnetic nanoparticles (MNP), which can be used in platforms for theranostics [20]. In [21], it was shown that ICG could be encapsulated in a polymer shell, which, in turn, could be electrostatically conjugated with monoclonal antibodies later on. These nanoscale capsules are suitable for both photodynamic therapy and tumor cell differentiation. In [22], nanoparticles of composites containing an amorphous matrix of calcium phosphate and silicon oxide with adsorbed ICG or FLN are shown. These composites were conjugated with monoclonal antibodies and were targeted delivered to various types of tumor cells. It was noted that the resulting composites can overcome the blood–brain barrier (BBB). Silicon oxide nanoparticles with adsorbed ICG could be represented as construction for theranostics since they have fluorescent and photoacoustic contrast and can be used for hyperthermia of tumors. In [23], chitosan-genipin nanoparticles in a PEG shell with inclusions of green indocyanine were developed for hyperthermia of tumors. Along with oncology, photodynamic therapy using ICG can be employed to treat actinic keratosis, infections, and acne [24].

However, the clinical use of ICG in high concentrations can cause side effects such as itching, hives, sweating, headache, and anaphylactic shock [25].

The review [26] shows that in 2011, the number of publications stored in the PubMed system concerning the use of ICG for imaging of tissue ischemia is four times less than the number of works that demonstrated the use of ICG in oncology and six times less than the number of works in the field of ophthalmology. The number of works using ICG in the field of phlebology and plastic surgery is growing rapidly [27].

Another fluorophore, and, at the same time, cardioprotector, that can be used in vivo is quinacrine (QIC), which is also called mepacrine and acrichine. QIC was synthesized in the 1930s of the twentieth century as a fluorescent dye. Its antimalarial and antiparasitic activities were soon discovered. In the last few decades, there have been articles showing a positive effect of mepacrine on postischemic myocardial recovery [28, 29]. When injected intravenously in certain doses (for rats >0.5 mg/kg per min), this fluorophore shows a strong hypotensive effect, so it is preferable to use quinacrine encapsulated in liposomes.

Since the discovery of the photoluminescence phenomena of porous silicon in 1990 [30], luminescent (porous) silicon nanoparticles have been obtained by several methods [31–35]. Some of them can be used biologically [34, 35]. Electrochemically etched porous silicon has a significant potential for biological applications due to its biocompatibility [36], biodegradability [37], encoding for multiplex detection [38], and tunable porous nanostructure and usage for drug delivery [39]. For in vivo applications, silicon nanoparticles have attractive physical, chemical, and biological properties compared to heavy metal-containing quantum dots, which have been shown to be toxic in biological environments. In addition, silicon is an important element in human organism, and the biodegradation product of porous silicon, orthosilicic acid ($\text{Si}(\text{OH})_4$), is a form absorbed by the human body and is naturally found in numerous tissues. In addition, silicic acid injected to humans is effectively excreted from the body with the urine [40].

This work presents in vitro and in vivo studies of the fluorescent dyes and luminescent porous silicon nanoparticles (PLPor-Si) using the IVIS Lumina III imager (PerkinElmer, USA). These objects are promising for theranostics applications, due to their ability for targeted drug delivery, and their own luminescence enables to control both the accumulation and the degradation of nanoparticles.

2. Synthesis and functionalization of nanomaterials

2.1 Immobilization of fluorescent dyes on the surface of nanoparticles

Fluorescent dyes are attached to nanoobjects for three different reasons. The first reason is an increased circulation time in the body. The second reason is caused by the fact that nanoobjects, due to their specific size, can stay in the ischemic area [41]. This enables to visualize the damage zone. The third and the most interesting reason is related to the possibility of simultaneous attachment of a fluorophore, a medicinal substance, and a guide ligand to nanoobjects. Such a nanoparticle turns into a theranostic structure [42].

Immobilization of fluorescent dyes on the surface of nanoparticles of any nature is carried out using an insertion—spacer molecule. For the chemical attachment of a fluorophore, the spacer must end with a functional group (**Figure 1**). Sometimes the material of the nanoparticle itself has a functional group, for instance, chitosan nanoparticles [43–45].

In practice, different types of spacers, ending in a functional group, are used. This occurs since the different fluorescent dyes have different functional groups and, hence, can react, that is, superstructure, on fragments of molecules ending in certain functional groups. For example, fluorophores that have acid groups in their composition (carboxyl, sulfo-, sulfonyl, and so on) are better immobilized to a radical that has an amino group, and vice versa, fluorescent dyes containing an amino group

easily interact with acid groups. Besides, there are spacers (e.g., glycerine) that can transform and form a covalent bond with a functional group (for instance, amino-). Moreover, they can be both primary and secondary amines.

For the spacer synthesis, its length is of great importance. For instance, the fluorophore, in order to avoid quenching the fluorescence, should be as far as possible remotened from the magnetic nanoparticle. This is regulated by the length of the insertion molecule, i.e., the spacer. To immobilize the fluorophores on magnetic nanoparticles, albumin can be used as a large protein with different functional groups and chitosan as a biopolymer with a large molecular weight (**Figure 2**).

Another popular method to prolong the action period of fluorophores is their encapsulation in liposomes (**Figure 3**). In addition, the liposome itself may contain a drug substance and a targeting ligand and serve as an object of theranostics [46].

Chitosan is one of the most promising biodegradable polymers. Chitosan-based nanoparticles are used for directed drug delivery [43–45]. Systems for the controlled release of medicines are being developed on the chitosan basis as well [47]. There is a fundamental opportunity of using chitosan nanoparticles (NPC) as markers for in vitro and in vivo imaging in those areas of the body, where the vascular permeability changes dramatically. For this purpose, they are coated with fluorescent dyes, such as indocyanine green, fluorescein, or colloidal quantum dots [48, 49].

Chitosan is a natural biopolymer, with every monomer containing a primary amino group. This makes it an extremely profitable material for the coordination-immobilization of fluorophores, which are organic acids (fluorescein and indocyanine green). The scheme of their immobilization is shown in **Figure 4**.

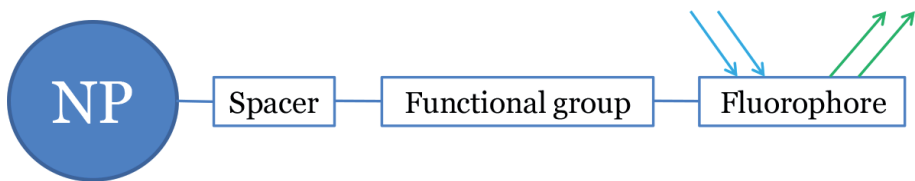


Figure 1.
Scheme of fluorophore immobilization on the nanoparticle surface.

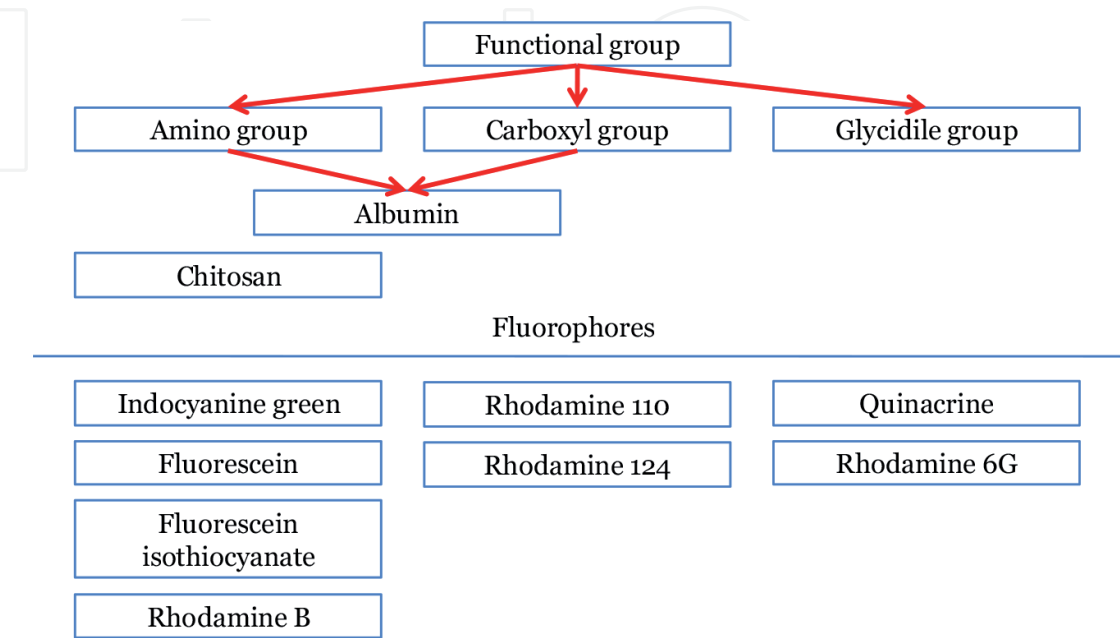


Figure 2.
Classification of functional groups and fluorophores.

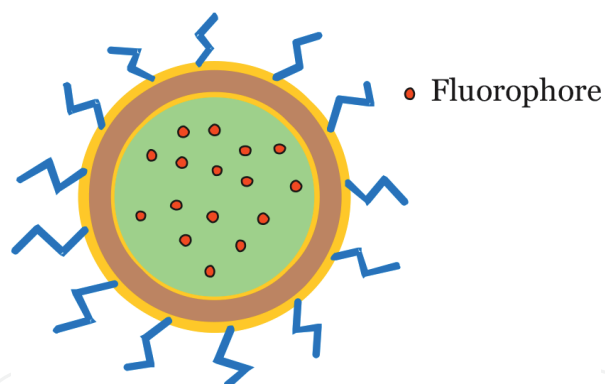


Figure 3.
Fluorophore in a liposomal form.

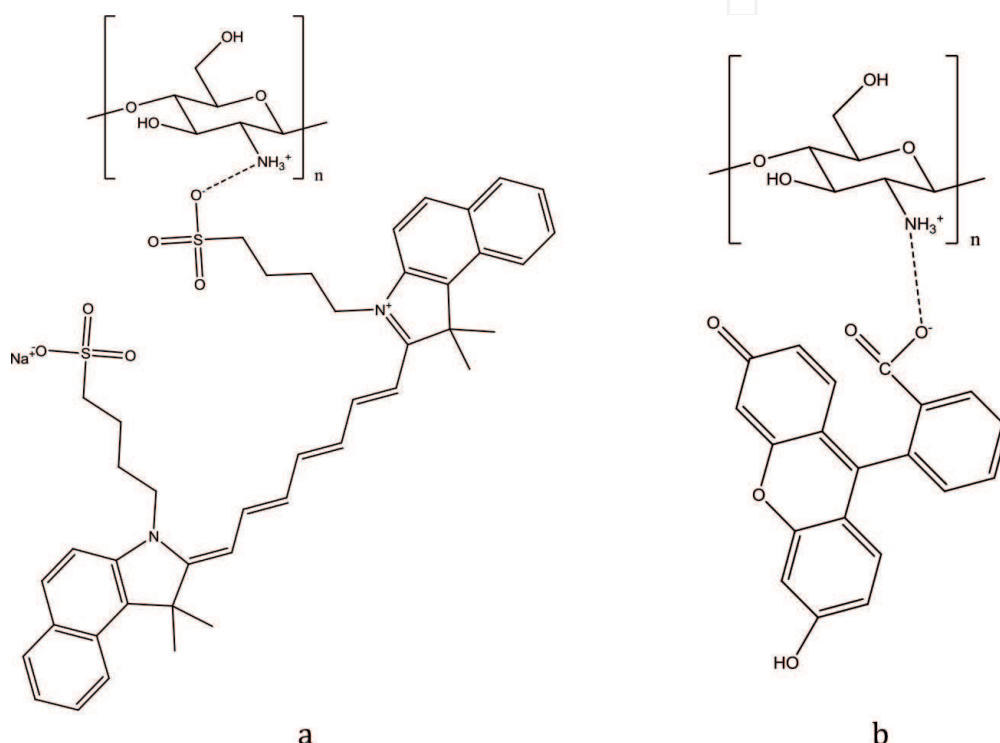


Figure 4.
Chitosan conjugation.

Thus, if one prepares nanoparticles from chitosan, it is possible to immobilize these fluorophores on them and get a fluorescent nanoagent.

If the nanoparticle does not contain a natural functional group, then it is synthesized on the surface.

The traditional method of such synthesis on the surface of functional amino group nanoparticles is the treatment of (3-aminopropyl)triethoxysilane (APTES). The reaction is usually conducted in an organic solvent at its boiling point with an intensive mixing [50]. Common solvents applied for the synthesis are benzene, toluene, cyclohexane, or monoatomic alcohols. APTES reacts with the hydroxylated surface of the nanoparticle (**Figure 5**). Since the hydroxylated surface is inherent for magnetite and silica nanoparticles, these nanoparticles are used for the amination of APTES.

Coordination-ion immobilization of FLN on the APTES-synthesized spacer gives an extremely weak chemical bond, which is hydrolyzed in aqueous solutions. Therefore, fluorescein is immobilized covalently using the carbodiimide method. **Figure 6** shows a method for immobilizing FLN using diisopropylcarbodiimide on a spacer obtained from APTES.

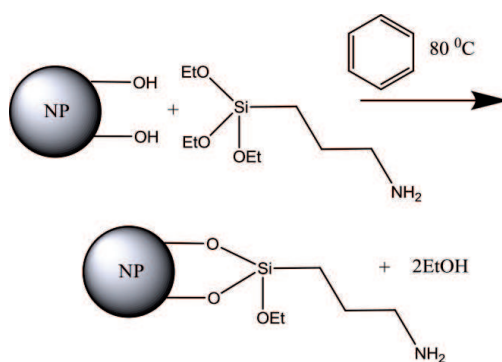


Figure 5.
The scheme of amino-spacer synthesis.

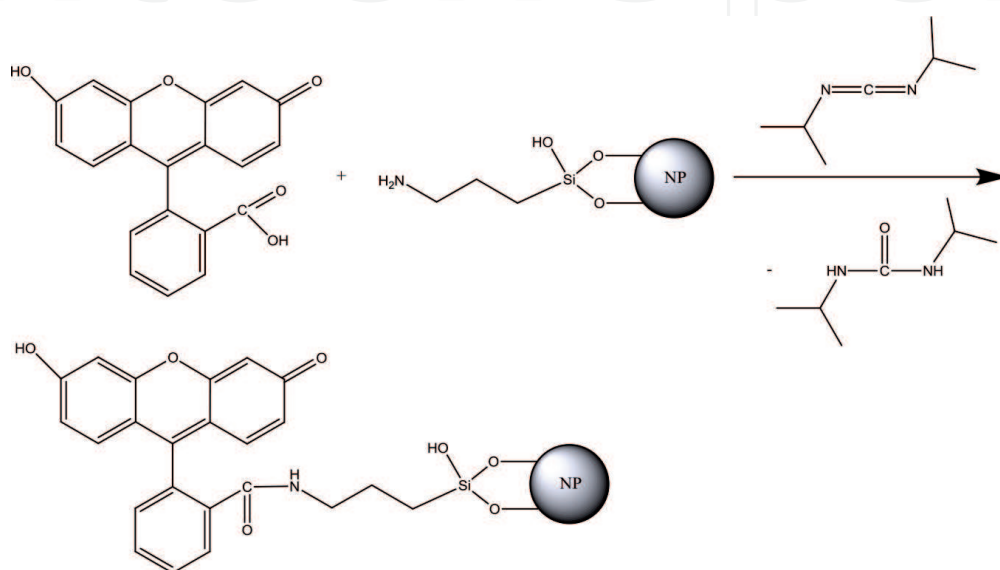


Figure 6.
Scheme of covalent immobilization of fluorescein on an amino spacer using diisopropylcarbodiimide (DIPC).

This is the simplest and most effective way to immobilize fluorescein on the surface of laminated nanoparticles. It is based on the application of the FLN—fluoresceinisothiocyanate (FITC) derivative. By processing nanoparticles with a spacer containing an amino group, under standard conditions in a dimethyl sulfoxide (DMSO) solvent, the amino group forms a covalent bond with the FITC isothiol group (**Figure 7**). The effectiveness of this immobilization is much higher than the reaction using FLN and DIPC. This was confirmed by the fluorescence measurements of the obtained samples. For FITC immobilization, it was 3.44×10^{11} [p/s]/ $[\mu\text{W}/\text{cm}^2]$ and for FLN immobilization using DIPC 1.01×10^{11} [p/s]/ $[\mu\text{W}/\text{cm}^2]$, respectively (**Figure 8**).

In contrast, while ICG is immobilized on an amine spacer obtained from APTES, the sulfogroup forms a strong ionic bond with the amine group, which can only be destroyed by an alcoholic solution of alkali. The scheme of such immobilization is demonstrated in **Figure 9**.

2.2 Synthesis of luminescent nanoparticles of porous silicon

Porous silicon layers were obtained by electrochemical etching of a single-crystal, (100)-oriented n-type silicon with a resistivity of 1–4.5 Ω/cm , at a constant current density of 40 mA/cm² for 20 min using an aqueous-alcohol electrolyte based on 48% hydrofluoric acid. The obtained porous film was removed by dipping

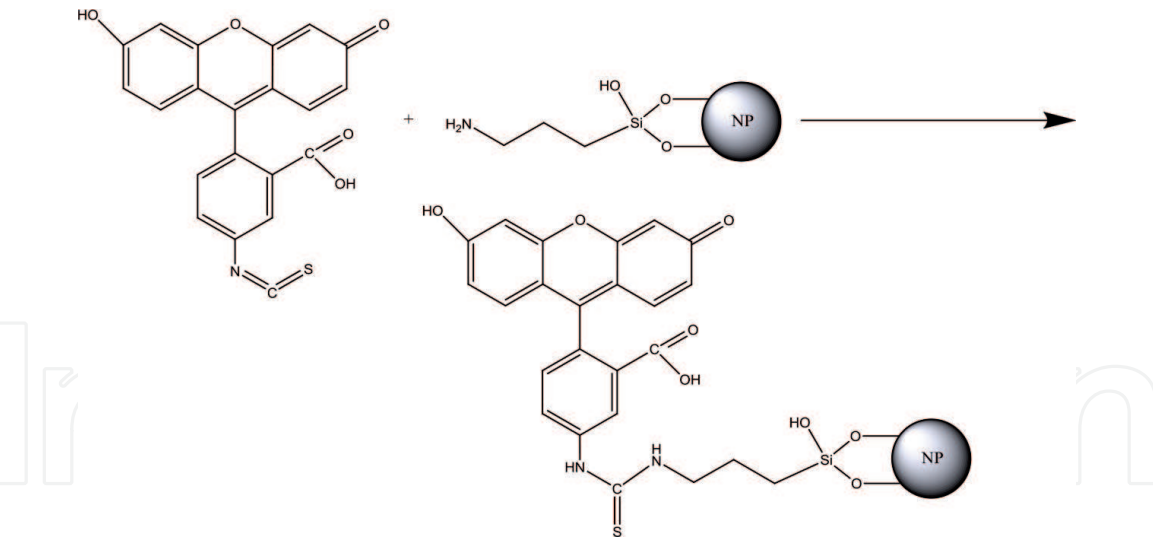


Figure 7.
Scheme of covalent immobilization of fluorescein isothiocyanate on an amino spacer.

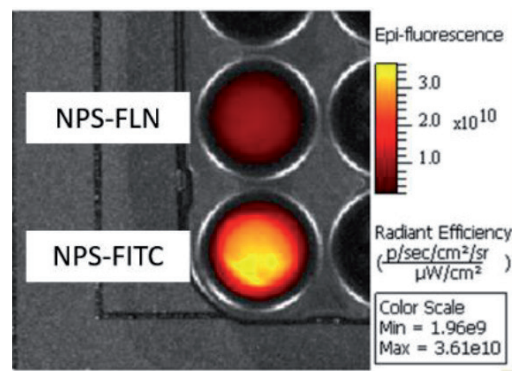


Figure 8.
Comparison of in vitro fluorescence FLN and FITC covalently immobilized on NPS.

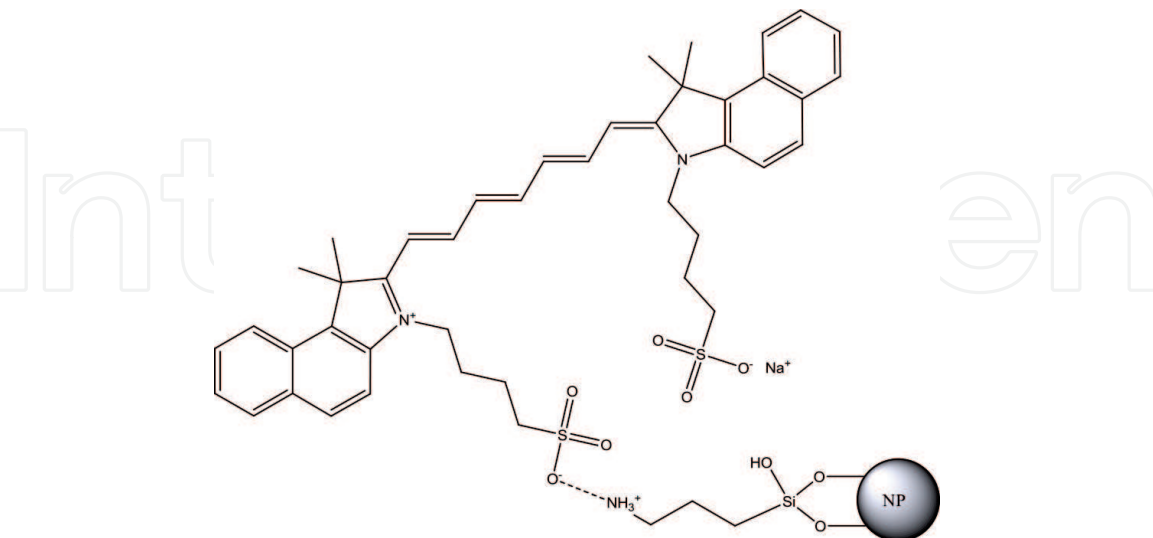


Figure 9.
Scheme of coordination-ion immobilization of green indocyanine on an amino spacer.

the plate in a solution with deionized water, with sequential exposure to ultrasound (“Saphir” ultrasound bath) for 30 min. The resulting suspension was filtered through the syringe filtration membranes (Millipore) with a diameter of less than 0.3 microns. The filtered suspension was further processed using a 600-watt local

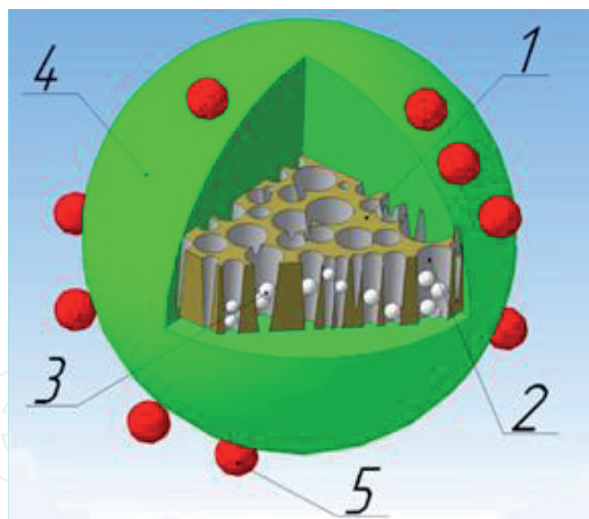


Figure 10.

Model of a system for targeted drug delivery based on photoluminescent porous silicon nanoparticles: (1) PLPor-Si nanoparticles; (2) oxidized layer (SiO_2 layer); (3) dosage form (payload); (4) biopolymer shell (dextran); (5) homing molecules (vitamin B₉).

ultrasonic homogenizer (SONOPULS) in an interval pulse mode for 30 min. At the next step, the particles were filtered through a 0.22- μm filtration membrane (Millipore). Afterwards, the nanoparticles were incubated in deionized water for ~2 weeks to activate their photoluminescent glow. To remove the dissolved silicic acids, the resulting dispersion was centrifuged at 13,000 rpm for 30 min, and a supernatant containing silicic acids and nanoparticles smaller than 20 nm in size was removed [51].

2.3 Functionalization of PLPor-Si nanoparticles with gentamicin

The functionalization of photoluminescent nanoparticles of porous silicon with gentamicin (PLPor-Si-Gent) was performed by impregnation: 0.5 ml of gentamicin solution (40 mg/ml) for an intravenous injection was added to 1.5 ml of the dispersion of porous silicon nanoparticles in deionized water. The sample was then subjected to ultrasound treatment for 15 min.

2.4 Functionalization of PLPor-Si nanoparticles with dextran

To cover the obtained photoluminescent nanoparticles derived in previous sections, a dextran shell with 1 ml of dispersion with nanoparticles (PLPor-Si or PLPor-Si-Gent) was used and mixed with 1 ml of aliquot of water containing 100 mg of dextran (MW ~20,000, Sigma). The mixture was stirred for 24 h and washed three times every 8 h using a centrifugal filter (100,000 molecular weight cutoff; Millipore) for the Eppendorf tube at 13,000 rpm for 30 min. The resulting nanoparticles (DPLPor-Si or DPLPor-Si-Gent) were poured into 2 ml Eppendorf tubes for the further injection to male rats of the Wistar stock. An example of a system for targeted drug delivery based on photoluminescent porous silicon nanoparticles is shown in **Figure 10**.

3. Characterization and study of fluorescence of PLPor-Si nanoparticles

Scanning electron microscopy (SEM) was used to control the morphology and the particle size of photoluminescent porous silicon using the Mira Tescan II

scanning electron microscope. The research was carried out with the detection of secondary and reflected electrons; the typical values of the accelerating voltage were 5–20 kV. Typical magnification values were in the range of 10,000–200,000. The control of the biodistribution and the study of the morphology of por-Si particles after internalization of the rats were performed on the liver and myocardial tissue fragments. Tissue samples were dried, and a thin layer of carbon was applied to the surface of the samples immediately before the SEM investigation [52].

To control and to verify the presence of photoluminescent PLPor-Si nanoparticles in the tissues after internalization, several experiments were previously performed on the injection of unloaded shell-free carriers (PLPor-Si) using a method similar to that for carrier particles loaded with medication (PLPor-Si-Gent) and coated with dextran (DPLPor-Si and DPLPor-Si-Gent) [53]. The study of the fragments of the rat's liver and heart tissues using the SEM method after an intravenous injection of por-Si particles (from the first set) revealed the presence of electron-dense particles with a shape close to spherical. It is worth noticing that the distribution of the particles in the tissues is uneven and the clusters of particles are observed near to the openings of the large ducts (**Figure 11**). The diameter of the detected particles corresponds well to the range of diameters of the first set of the particles: 60–80 nm the main part of the particles, with some larger (up to 185 nm) particles and a fraction of the smaller particles (≈ 30 –40 nm).

The photon cross-correlation method (PCCS) was employed to determine the size of nanoparticles obtained using the Nanophox analyzer from Sympatec (Germany). Before the dispersion measurement procedure, the samples were further broken up with a 600-W ultrasonic homogenizer for 5 min. Later on, the solutions with a mechanical dispenser were taken and poured into the cuvette of the analyzer. The concentration of solutions was selected in a way that the average intensity of the scattered light for each sample was the same. The absence of multiple light scattering was visually controlled. The processing was performed with the DynaLS software: correlator channels from 30 to 200 and search boundaries from 1 to 10,000 nm. **Table 1** shows the size distribution of the nanoparticles from sets 1 to 4 determined by photon cross-correlation spectroscopy.

The study of the photoluminescence of the samples of porous silicon nanoparticles (PLPor-Si, PLPor-Si-Gent, DPLPor-Si, DPLPor-Si-Gent) obtained in the work was conducted at room temperature using an automated spectral complex assembled based on the MDR_23 and FEU_79 monochromator operating in the

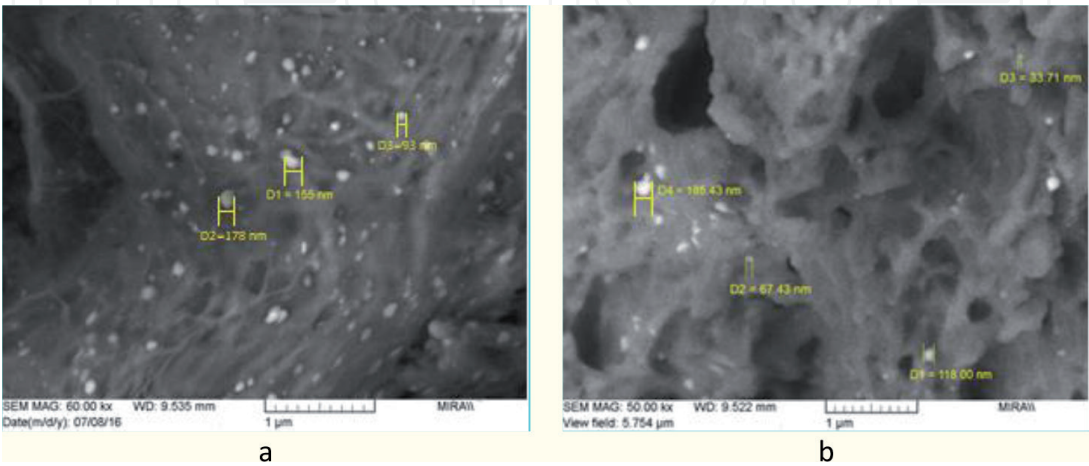


Figure 11. Rat's heart tissue (myocardium) (a) and liver (b) at a single magnification. Diffuse distribution of electron-dense centers with the size corresponding to the size of the particles from injected dispersion PLPor-Si of the first set (80–190 nm).

photon-counting mode. Photoluminescence was excited by the radiation with a wavelength of 405 nm. **Figure 12** shows the photoluminescence spectra obtained during the experiment 5 days after receiving.

One can see that the process of functionalization of nanoparticles (PLPor-Si) leads to a redistribution of intensity in the photoluminescence band of the initial samples from the first set with almost complete preservation of its position and

Number of the sets		Synthesis conditions				Diameter of the particles (nm)	
		Silicon type	J_A , mA/cm ²	t_A , min	t_{US} , min	Value	Measuring method
1	PLPor-Si	n-Si	40	20	30	≈20–190	PCCS SEM
2	DPLPor-Si					≈250–300	PCCS
3	PLPor-Si-Gent					≈180–250	
4	DPLPor-Si-Gent					≈250–330	

Table 1.
Conditions of the synthesis and the parameters of the silicon porous nanoparticles.

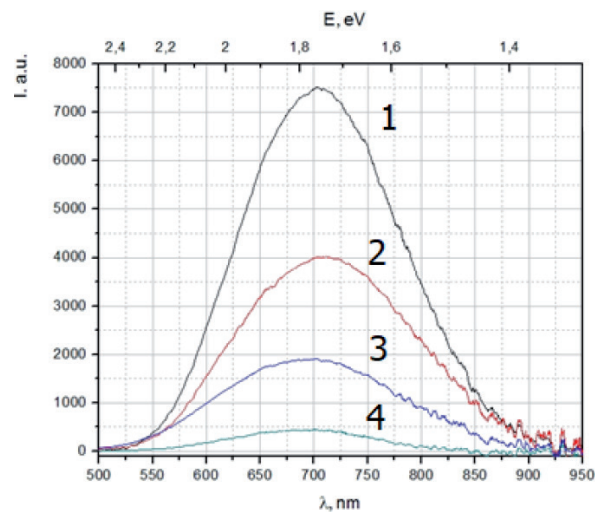


Figure 12.
The photoluminescence spectra: (1) PLPor-Si; (2) DPLPor-Si; (3) PLPor-Si-gent; and (4) DPLPor-Si-gent.

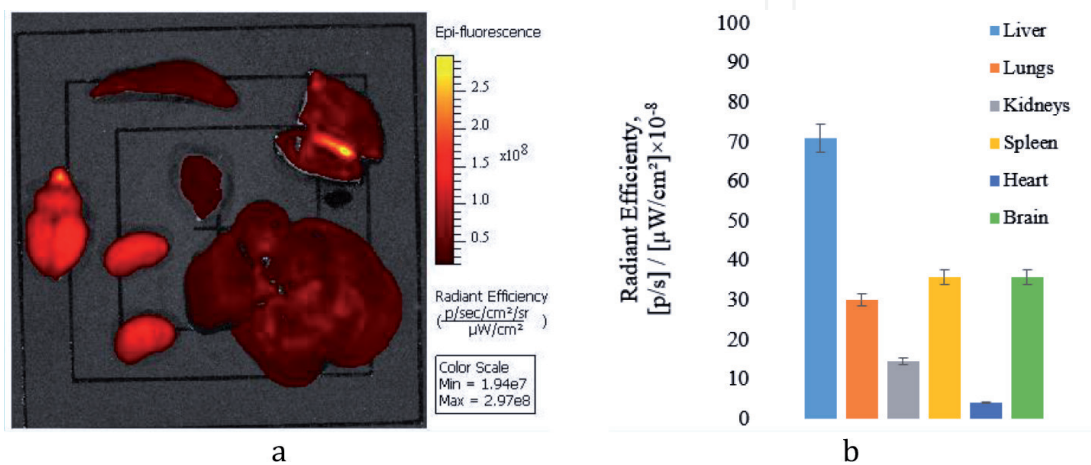


Figure 13.
Detection of PLPor-Si (second series) ex vivo (a); fluorescence intensity of the rat's organs (b).

width. Coating of the second set of samples with the dextran-2 (DPLPor-Si) drives to the formation of a thicker surface layer, which, in turn, causes a decrease in the intensity of FL almost twice as compared to the original samples from the first set. The functionalization of the surface of nanoparticles by the drug (gentamicin) third set (PLPor-Si-Gent) leads to a more intensive passivation of the surface by the drug molecules, which reduces the intensity of the photoluminescence line by more than three times. The combination of drug and dextran functionalization methods for the fourth set of samples (DPLPor-Si-Gent) reduces the luminescence intensity by an order of magnitude, due to a significant increase in the surface layer and passivation of the surface by drug molecules.

The fluorescent emission was measured using a fluorescent imager IVIS Lumina LT III (PerkinElmer, USA). To investigate the overall biodistribution and potential application of DPLPor-Si, a 1-ml solution with 0.5 mg/ml concentration of DPLPor-Si was injected into the tail vein of a Wistar stock rat. After 24 h from the moment of injection, the organs were removed for evaluation. Fluorescent emission was recorded on the standard embedded filters (for excitation, 500 nm, and for emission, 650 nm). **Figure 13** demonstrates the fluorescent analysis of ex vivo organ distribution in a male Wistar rat 24 h after an intravenous injection of the nanoparticles from second set.

Ex vivo organ biodistribution presents a steady accumulation of DPLPor-Si nanoparticles in the liver (**Figure 13b**). It is important to mention that after the intravenous injection, DPLPor-Si penetrates the blood–brain barrier and there is retention of the particles in the brain. Such particles have great potential for research in the fields of neurology and neurosurgery.

4. Use of fluorophore-labeled nanoparticles for fluorescent imaging in preclinical studies

Fluorescence of nanoparticles was measured using a fluorescence imager. Herein, **Figure 14a** shows a photograph of fluorescein (left) and indocyanine green (right) immobilized on chitosan microparticles. As can be seen, the fluorophores are completely chemisorbed on the particles, and the chemical bond with chitosan amino groups is not hydrolyzed, which is confirmed by the absence of a free dye in the solution.

Figure 14b reveals a samples' image taken with the IVIS Lumina LT fluorescent tomography in “spectral unmixed” mode. This mode allows to take multiple frames with different excitation wavelengths and various registration cutoff filters with a consequent combination as a result. Samples are shown from left to right: chitosan particles without fluorophore, particles with FLN, and particles with ICG. To induce fluorescence the embedded light filters were used (for FLN, 465 nm, and for ICG, 745 nm). Registration was performed with built-in FITS and ICG filters, respectively, suitable for the release of induced radiation of the corresponding fluorescent dyes and following the documentation for the device.

The use of nanoparticles labeled with different fluorophores enables to simultaneously or sequentially introduce them into the body of laboratory animals and study their biodistribution. Moreover, particles with different size and origin can be labeled with different fluorophores and examined simultaneously. As a demonstration of this, a Petri dish with the organs of laboratory animals obtained on a fluorescent tomography in the “spectral unmixed” mode is shown in **Figure 15**. Before euthanasia and removal of the organs, the animal underwent an intravenous injection of the suspension with the nanoparticles of chitosan labeled with fluorescein and indocyanine green consistently.

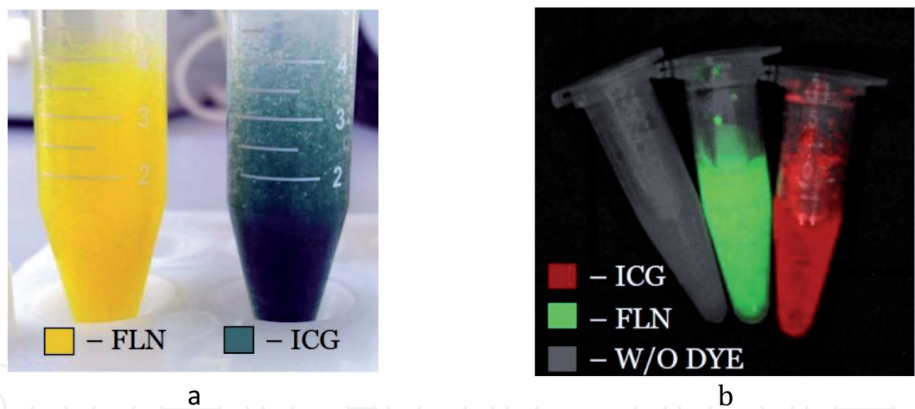


Figure 14. Image of chitosan microparticles with immobilized fluorescein (FLN) and indocyanine green (ICG): (a) in daylight; (b) on a fluorescent tomography of samples in comparison with a control sample without dye in the “spectral unmixed” mode.

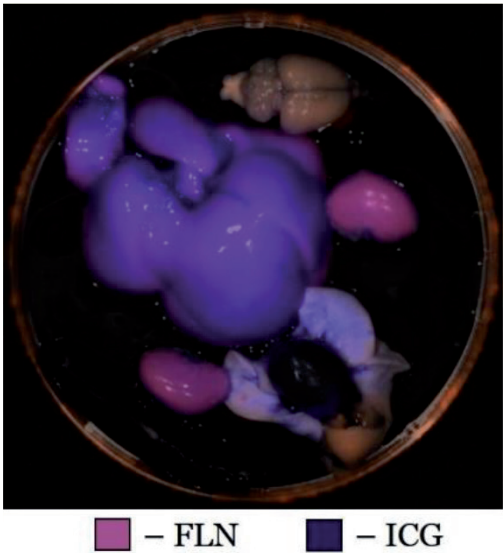


Figure 15. Rat’s organs, after the introduction of chitosan nanoparticles labeled with fluorescein and indocyanine green; image from a fluorescent tomography in the “spectral unmixed” mode.

It is worth noticing that nanoparticles labeled with fluorescein are mainly visible in the kidneys while particles labeled with green indocyanine are localized in the liver and lungs. Chitosan nanoparticles labeled with fluorophores do not overcome the blood–brain barrier. At the same time, one can see that only the autofluorescence inherent to NADH is visible in the brain.

The biodistribution of chitosan nanoparticles in vivo was evaluated over a period of 30 min. The following time intervals were selected: initial state, 5, 10, 15, 20, 25, and 30 min. After catheterization of the femoral vein of the laboratory animal, NPC-ICG was injected. In other words, the image registration in each animal was performed initially, before the introduction of suspensions, 5 min after the introduction, and then every 5 min for half an hour (**Figure 16a**). Afterwards, the animals were removed from the experiment by increasing the dose of anesthetic and removing the organs for examination: heart, lungs, liver, spleen, and kidneys.

The evaluation of the biodistribution based on the obtained fluorescence in vivo from the surface of the entire animal body revealed a maximum accumulation of the nanoparticles had occurred only in one area of the body (**Figure 16a**) with the increase of the intensity at the same area with time (**Figure 16b**). An autopsy of the animal and the removal of the listed organs, which were placed in a Petri dish with

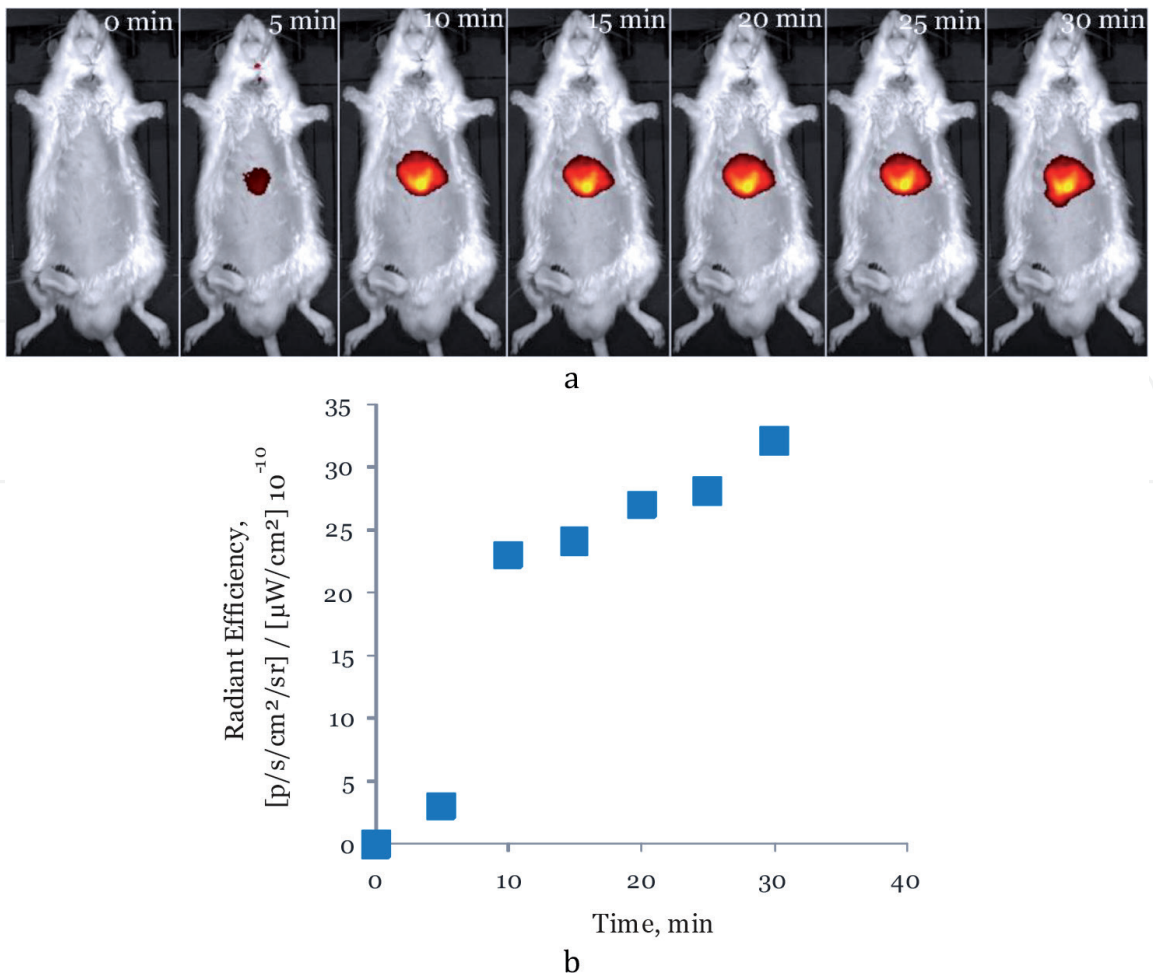


Figure 16. Fluorescent imaging in vivo distribution NPC-ICG administered intravenously (a); the dependence of the fluorescence intensity distribution on time (b).

consequent analysis on a fluorescent imager, were performed. It was found that the greatest accumulation of NPC-ICG particles occurred in the liver (**Figure 17**). As expected, the data indicates the elimination of nanoobjects by the liver and confirms the previously obtained data using histochemical staining by Grocott on the predominant accumulation of NPC in the rats' liver [54].

Male rats from Wistar were used to estimate the overall biodistribution of NPS-FLN and liposomal quinacrine drug (LQD). NPS-FLN and LQD solutions with a volume of 2 ml were injected intravenously through the tail vein; then the animals were anesthetized with isoflurane anesthesia and placed in the fluorescent analyzer. As for negative control, a rat given with an intravenous saline solution of 2 ml volume was used. The in vivo visualization of the biodistribution was recorded every 5 min for 30 min (**Figure 18**). After removing the animals from the experiment by humane euthanasia with an overdose of inhaled anesthesia of isoflurane, organ sampling was performed (**Figure 19**) for ex vivo quantification of particle accumulation. The fluorescence intensity from the area of interest (ROI) was calculated using the Living Image software (Living Image 4.5.5, PerkinElmer Inc.).

After the evaluation of the overall in vivo distribution of NPS-FLN nanoparticles over time, no local areas of fluorescence accumulation were found. The same situation was observed in the case of the LQD sample. As expected, that happened because fluorescein (ex, 490 nm; em, 525 nm) and quinacrine (ex, 490 nm; em, 525 nm) had the same wavelength of radiation, which was damped by autofluorescence of the biological tissues. Therefore, such fluorescent dyes are more often used for ex vivo and in vitro evaluation.

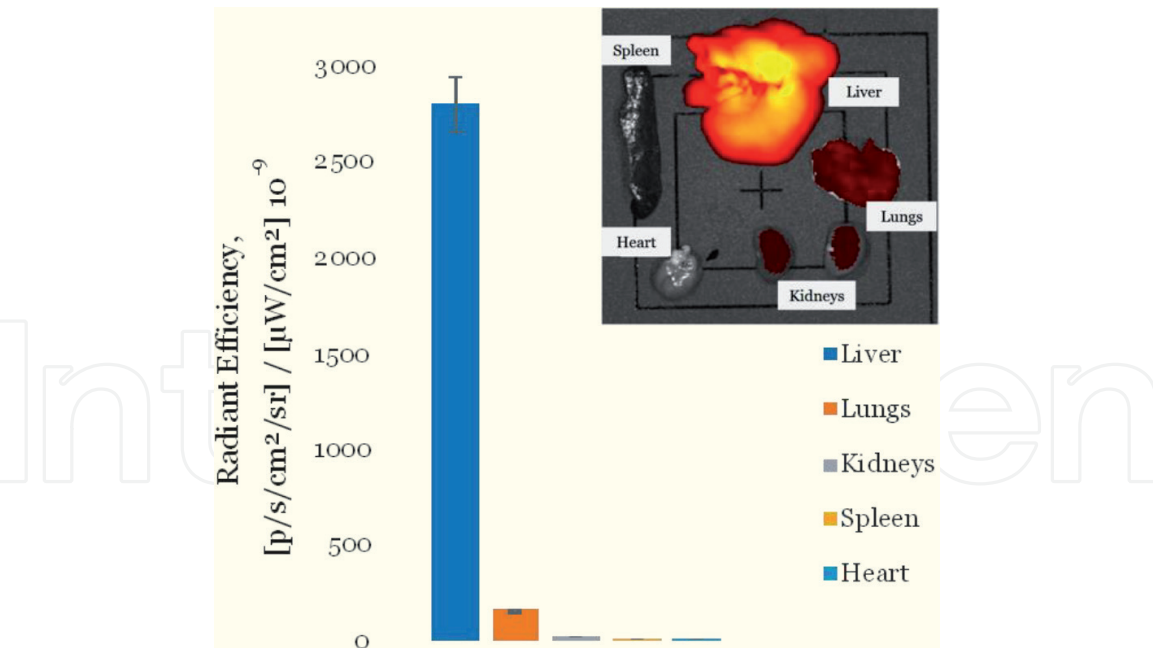


Figure 17. Images ex vivo and fluorescence intensity of the five major organs, liver, lungs, kidneys, spleen, and heart seized from the rat with introduced NPS-ICG.

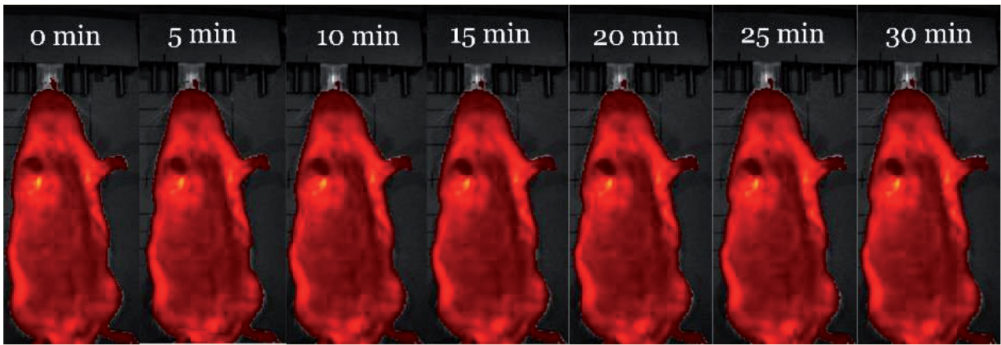


Figure 18. Fluorescent imaging in vivo distribution NPS-FLN administered intravenously.

The quantitative biodistribution of the intensity of the fluorescent glow NPS-FLN and LQD in the bodies is illustrated in **Tables 2** and **3**. The accumulation of NPS-FLN particles mainly occurs in the liver, lungs, spleen, and kidneys. In the case of LQD, accumulation was observed in the lungs, which is justified by the size of the liposomes themselves, the average size of which is $1 \mu m$. The accumulation or deposition of liposomal points occurs by mechanical filtration through the capillary channel of the lung after an intravenous injection [55, 56].

The NPC-ICG biodistribution study (**Figure 20**) was conducted similarly to the one presented above. Another fluorescent dye (ICG) with the emission outside the autofluorescence of the tissue range was used, so the emission falls into the transparency window of biological objects [57–59].

Depending on the method of intravenous injection of nanoparticles conjugated with the fluorescent dye ICG, a significant difference in the estimation of the fluorescence intensity of the total biodistribution over time is observed. For example, when the NPC-ICG conjugate is directly inserted into the catheterized femoral artery, there is an increase in the intensity of the fluorescent glow in the liver region over time (**Figure 16a**). On the other hand, intravenous injection through the tail vein (**Figure 20**) causes a general glow of the entire surface of the animal. After 5 min, and then during the entire experiment, an accumulation of nanoparticles

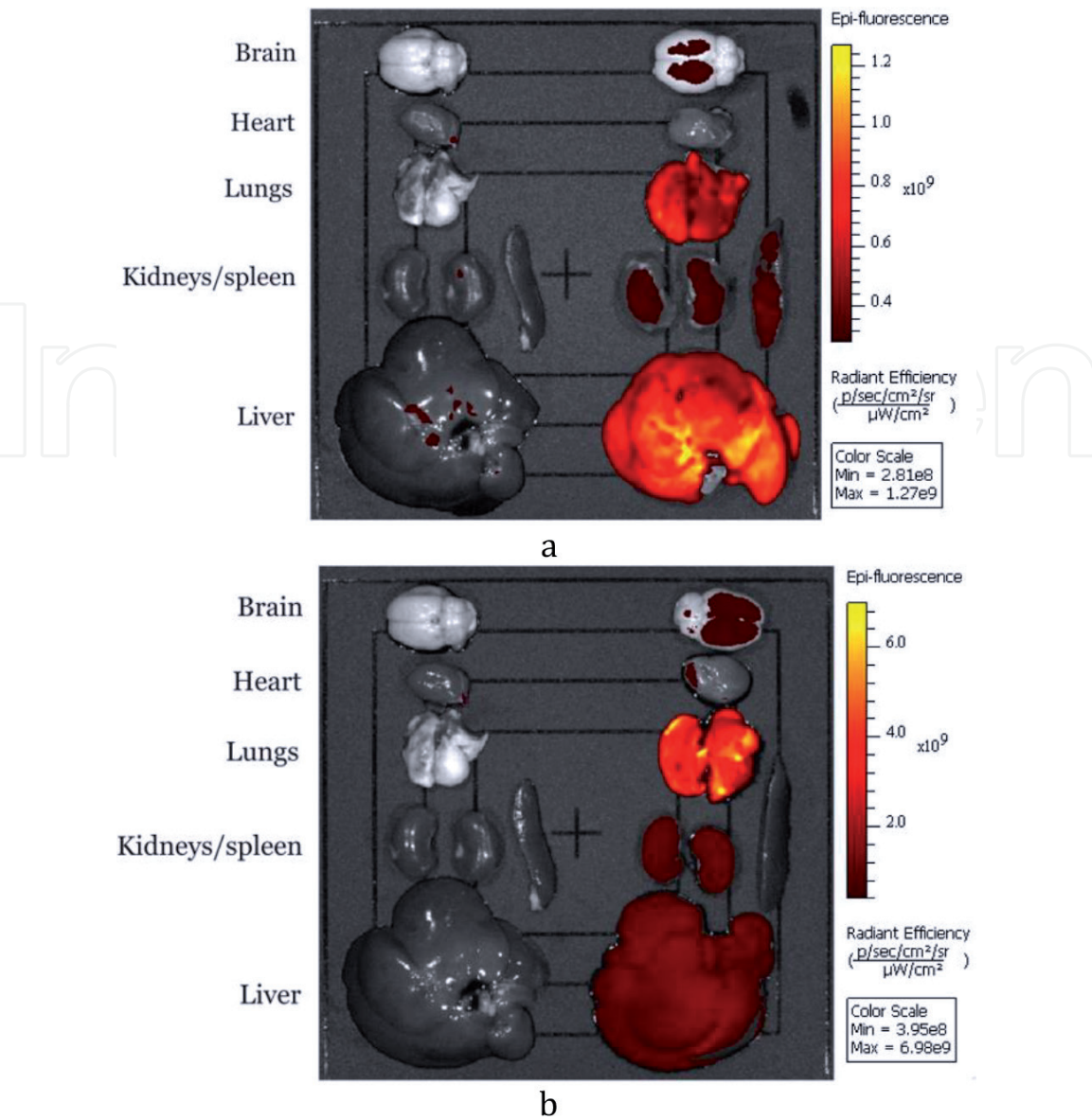


Figure 19.
Ex vivo fluorescence intensity of the five major organs, liver, lungs, kidneys, spleen, and heart seized from the rat with introduced NPS-FLN (a) and LQD (b).

Organ	Total radiant efficiency [p/s]/[μW/cm ²] × 10 ⁻⁹		
	Control	NPS-FLN	The difference with the control
Brain	1.56	6.55	4.99
Heart	0.94	1.25	0.31
Lungs	1.56	25.50	23.94
Kidneys	3.01	5.23	2.22
Spleen	0.82	6.72	5.90
Liver	25.00	108.00	83.00

Table 2.
Total radiant efficiency of organs with control and with introduced NPS-FLN.

in the liver occurs, and a decrease in the intensity of fluorescence (**Figure 20b**) takes place. As shown in the previous experiment on NPS-ICG biodistribution, the accumulation of such conjugates occurs in the liver, lungs, kidneys, and spleen.

Organ	Total radiant efficiency [p/s]/[μW/cm ²] × 10 ⁻⁹		
	Control	LQD	The difference with the control
Brain	4.39	14.10	9.71
Heart	1.16	3.91	2.75
Lungs	1.56	169.00	167.44
Kidneys	2.95	16.40	13.45
Spleen	1.02	1.97	0.95
Liver	27.80	207.00	179.2

Table 3.
Total radiant efficiency of organs with control and with introduced LQD.

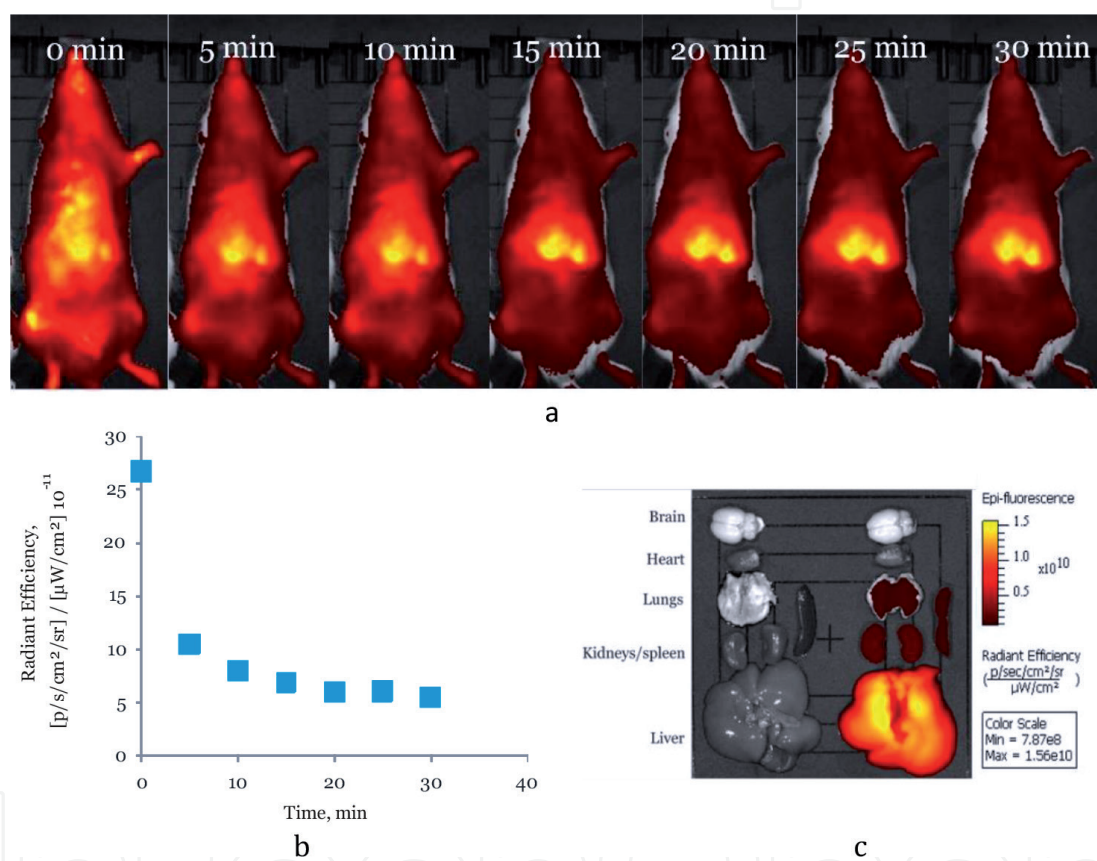


Figure 20.
Fluorescent imaging in vivo distribution of NPS-ICG administered intravenously (a); the dependence of the fluorescence intensity distribution on time (b); ex vivo biodistribution of NPS-ICG (c).

Organ	Total radiant efficiency [p/s]/[μW/cm ²] × 10 ⁻⁹		
	Control	NPS-ICG	The difference with the control
Brain	3.01	4.47	1.46
Heart	1.55	2.62	1.07
Lungs	5.85	46.40	40.55
Kidneys	1.02	32.40	31.38
Spleen	2.67	21.30	18.63
Liver	12.80	2240.00	2227.20

Table 4.
Total radiant efficiency of organs with control and with introduced NPS-ICG.

Ex vivo biodistribution in organs shows the accumulation of the particles mostly in the liver. The numerical distribution of NPS-ICG accumulation is shown in **Table 4**.

It is important to mention that nanoparticles conjugated with the fluorescent dye ICG are suitable for in vivo visualization of biodistribution and accumulation in the area of interest since its emission lies in the transparency window of biological tissues [60, 61]. Further modification and creation of agents for theranostic based on such dyes is promising for fluorescence tomography in preclinical studies.

5. Conclusion

Nanomaterials conjugated with fluorophores have a great perspective for application of in vitro and in vivo fluorescence tomography in preclinical studies on laboratory animals. In comparison with pure fluorophores, they have several advantages. First, these conjugates have the effect of prolongation allowing performing a visualization for at least 30 min. Non-bound fluorophores can metabolize within 1–2 min. Second, the usage of nanoparticles of different nature and physical size enables the visualization of different organs, due to their accumulation in different parts of the body. Finally, such conjugates can be used to create platforms for theranostics, which will suit well for the early diagnosis and therapy for use in personalized medicine.

Local drug delivery systems based on the photoluminescent nanoparticles of porous silicon (PLPor-Si) obtained by electrochemical anodic etching were developed. The developed functionalization methods allowed the encapsulation of the photoluminescent nanoparticles on a porous silicon basis with the drug gentamicin (PLPor-Si-Gent) and obtaining the shell systems for local drug delivery using a biocompatible dextran polymer (DPLPor-Si or DPLPor-Si-Gent).

Photon cross-correlation spectroscopy applied to a series of porous silicon samples before the internalization determined the average size of the particles. For instance, for the samples of first series (PLPor-Si), the average size of the hydrodynamic diameter of the studied nanoparticle dispersions was determined by a range from 20 to 190 nm, which is confirmed by the measurements of the scanning electron microscopy of this series. The analysis of the fragments of the rat's liver and heart tissue performed by the SEM method after an intravenous injection of the first set nanoparticles yielded the presence of electron-dense particles with a shape close to spherical. The distribution in the tissues was nonuniform with the clusters observed near to the openings of the large ducts. The diameter of the detected particles corresponds well to the range of diameters of the first set particles: the major part of the particles (60–80 nm), with some larger (up to 185 nm) particles and a fraction of smaller particles (≈ 30 –40 nm).

The functionalization processes of the porous silicon nanoparticles with the molecules of the drug gentamicin and the dextran-based shell structure led to an increase in the average hydrodynamic diameter of the studied samples of second, third, and fourth sets. In this case, smaller particles aggregated to the following systems (herein the range of average hydrodynamic diameters): 250–300, 180–250, and 250–330 nm for second (DPLPor-Si), third (PLPor-Si-Gent), and fourth (DPLPor-Si-Gent) sample sets, respectively.

The photoluminescence spectra of the samples obtained in this work showed a process of functionalization of the nanoparticles (PLPor-Si). It drove to a redistribution of intensity in the photoluminescence band of the initial samples from set 1 with almost complete preservation of its position and width, at which the peak of the spectra fell in the wavelength range from 700 to 710 nm.

The samples coated with the dextran-2 (DPLPor-Si) form a thicker surface layer, which results in a decrease in the intensity of FL almost twice as compared to the

original first set. The functionalization of the surface of nanoparticles with the drug (gentamicin) third sets (PLPor-Si-Gent) entails the more intensive passivation of the surface by the drug molecules, which reduces the intensity of the photoluminescence line by more than (a) factor of 3. The combination of drug and dextran functionalization methods for samples from the fourth set (DPLPor-Si-Gent) dramatically reduces the luminescence intensity (by an order of magnitude), due to a significant increase in the surface layer and passivation of the surface by drug molecules.

The analysis of the biodistribution in the organs of male rats of the Wistar stock obtained by fluorescence spectroscopy of the samples from the second set after the internalization process showed an intense accumulation of DPLPor-Si nanoparticles in the liver, which in turn correlates with the data of scanning electron microscopy for these samples. After intravenous injection, DPLPor-Si penetrates the blood-brain barrier, and the particles concentrate in the brain.

Thus, the resulting local drug delivery systems which are able to circulate in the body have a huge potential for the diagnosis and treatment of various diseases. Such systems have a vast list of advantages like the ability to safely remove from the body for a given period of time after they perform their diagnostic or therapeutic function, the capability to be detected in vivo, a low level of toxicity, and a potential to overcome various complex barriers within the body, such as histohematic.

Conflict of interest

The authors declare no conflict of interest.

Author details

Dmitry Korolev^{1,2}, Maria Istomina^{1,3*}, Anton Belorus³, Artem Brovko⁴, Dmitry Sonin^{1,2}, Galina Shulmeyster¹, Natalya Evreinova^{1,5} and Vyacheslav Moshnikov³

1 Almazov National Medical Research Centre, Saint Petersburg, Russia

2 Pavlov First Saint Petersburg State Medical University, Saint Petersburg, Russia


3 Saint Petersburg Electrotechnical University "LETI", Saint Petersburg, Russia

4 Tel Aviv University, Tel Aviv, Israel

5 Saint Petersburg State Institute of Technology, Saint Petersburg, Russia

*Address all correspondence to: ist_maria@mail.ru

IntechOpen

© 2020 The Author(s). Licensee IntechOpen. Distributed under the terms of the Creative Commons Attribution - NonCommercial 4.0 License (<https://creativecommons.org/licenses/by-nc/4.0/>), which permits use, distribution and reproduction for non-commercial purposes, provided the original is properly cited. 

References

- [1] Wu Q, Merchant FA, Castleman KR. *Microscope Image Processing*. New York: Academic Press; 2008
- [2] Pic E, Pons T, Bezdetnaya L, Leroux A, Guillemin F, Dubertret B, et al. Fluorescence imaging and whole-body biodistribution of near-infrared-emitting quantum dots after subcutaneous injection for regional lymph node mapping in mice. *Molecular Imaging and Biology*. 2010;12:394-405. DOI: 10.1007/s11307-009-0288-y
- [3] Walsh EM, Cole D, Tipirneni KE, Bland KI, Udayakumar N, Kasten BB, et al. Fluorescence imaging of nerves during surgery. *Annals of Surgery*. 2019;270:69-76. DOI: 10.1097/SLA.0000000000003130
- [4] Jung JS, Jo D, Jo G, Hyun H. Near-infrared contrast agents for bone-targeted imaging. *Tissue Engineering and Regenerative Medicine*. 2019;16:443-450. DOI: 10.1007/s13770-019-00208-9
- [5] Lichtman JW, Conchello JA. Fluorescence microscopy. *Nature Methods*. 2005;2:910-919. DOI: 10.1038/nmeth817
- [6] Rao J, Dragulescu-Andrasi A, Yao H. Fluorescence imaging in vivo: Recent advances. *Current Opinion in Biotechnology*. 2007;18:17-25. DOI: 10.1016/j.copbio.2007.01.003
- [7] Etrych T, Lucas H, Janoušková O, Chytil P, Mueller T, Mäder K. Fluorescence optical imaging in anticancer drug delivery. *Journal of Controlled Release*. 2016;226:168-181. DOI: 10.1016/j.jconrel.2016.02.022
- [8] Kobayashi H, Ogawa M, Alford R, Choyke PL, Urano Y. New strategies for fluorescent probe design in medical diagnostic imaging. *Chemical Reviews*. 2010;110:2620-2640. DOI: 10.1021/cr900263j
- [9] Butner RW, McPherson AR. Adverse reactions in intravenous fluorescein angiography. *Annals of Ophthalmology*. 1983;15:1084-1086
- [10] Ntziachristos V. Fluorescence molecular imaging. *Annual Review of Biomedical Engineering*. 2006;8:1-33. DOI: 10.1146/annurev.bioeng.8.061505.095831
- [11] Neri D, Carnemolla B, Nissim A, Leprini A, Querzè G, Balza E, et al. Targeting by affinity-matured recombinant antibody fragments of an angiogenesis associated fibronectin isoform. *Nature Biotechnology*. 1997;15:1271-1275. DOI: 10.1038/nbt1197-1271
- [12] Weissleder R, Tung CH, Mahmood U, Bogdanov A. In vivo imaging of tumors with protease-activated near-infrared fluorescent probes. *Nature Biotechnology*. 1999;17:375-378. DOI: 10.1038/7933
- [13] Sonin D, Papayan G, Pochkaeva E, Chefu S, Minasian S, Kurapeev D, et al. In vivo visualization and ex vivo quantification of experimental myocardial infarction by indocyanine green fluorescence imaging. *Biomedical Optics Express*. 2017;8:151. DOI: 10.1364/boe.8.000151
- [14] Ogawa M, Kosaka N, Choyke PL, Kobayashi H. In vivo molecular imaging of cancer with a quenching near-infrared fluorescent probe using conjugates of monoclonal antibodies and indocyanine green. *Cancer Research*. 2009;69:1268-1272. DOI: 10.1158/0008-5472.CAN-08-3116
- [15] Papayan GV, Akopov AL. Fluorescence diagnostics in the near-IR: Apparatus, application. *Journal of Optical Technology*. 2016;83:536. DOI: 10.1364/jot.83.000536

- [16] Proulx ST, Luciani P, Derzsi S, Rinderknecht M, Mumprecht V, Leroux JC, et al. Quantitative imaging of lymphatic function with liposomal indocyanine green. *Cancer Research*. 2010;**70**:7053-7062. DOI: 10.1158/0008-5472.CAN-10-0271
- [17] Portnoy E, Lecht S, Lazarovici P, Danino D, Magdassi S. Cetuximab-labeled liposomes containing near-infrared probe for in vivo imaging. *Nanomedicine: Nanotechnology, Biology, and Medicine*. 2011;**7**:480-488. DOI: 10.1016/j.nano.2011.01.001
- [18] Beziere N, Lozano N, Nunes A, Salichs J, Queiros D, Kostarelos K, et al. Dynamic imaging of pegylated indocyanine green (ICG) liposomes within the tumor microenvironment using multi-spectral optoacoustic tomography (MSOT). *Biomaterials*. 2015;**37**:415-424. DOI: 10.1016/j.biomaterials.2014.10.014
- [19] Kraft JC, Ho RJY. Interactions of indocyanine green and lipid in enhancing near-infrared fluorescence properties: The basis for near-infrared imaging in vivo. *Biochemistry*. 2014;**53**:1275-1283. DOI: 10.1021/bi500021j
- [20] Muthu MS, Leong DT, Mei L, Feng SS. Nanotheranostics—Application and further development of nanomedicine strategies for advanced theranostics. *Theranostics*. 2014;**4**:660-677. DOI: 10.7150/thno.8698
- [21] Yu J, Javier D, Yaseen MA, Nitin N, Richards-Kortum R, Anvari B, et al. Self-assembly synthesis, tumor cell targeting, and photothermal capabilities of antibody-coated indocyanine green nanocapsules. *Journal of the American Chemical Society*. 2010;**132**:1929-1938. DOI: 10.1021/ja908139y
- [22] Barth BM, Sharma R, Altinoğlu EI, Morgan TT, Shanmugavelandy SS, Kaiser JM, et al. Bioconjugation of calcium phosphosilicate composite nanoparticles for selective targeting of human breast and pancreatic cancers in vivo. *ACS Nano*. 2010;**4**:1279-1287. DOI: 10.1021/nn901297q
- [23] Song X, Wu H, Li S, Wang Y, Ma X, Tan M. Ultrasmall chitosan-genipin nanocarriers fabricated from reverse microemulsion process for tumor photothermal therapy in mice. *Biomacromolecules*. 2015;**16**:2080-2090. DOI: 10.1021/acs.biomac.5b00511
- [24] Giraudeau C, Moussaron A, Stallivieri A, Mordon S, Frochot C. Indocyanine green: Photosensitizer or chromophore? Still a debate. *Current Medicinal Chemistry*. 2014;**21**:1871-1897. DOI: 10.2174/0929867321666131218095802
- [25] Kaiser M, Yafi A, Cinat M, Choi B, Durkin AJ. Noninvasive assessment of burn wound severity using optical technology: A review of current and future modalities. *Burns*. 2011;**37**:377-386. DOI: 10.1016/j.burns.2010.11.012
- [26] Alander JT, Kaartinen I, Laakso A, Pätälä T, Spillmann T, Tuchin VV, et al. A review of indocyanine green fluorescent imaging in surgery. *International Journal of Biomedical Imaging*. 2012;**2012**:1-26. DOI: 10.1155/2012/940585
- [27] Marshall MV, Rasmussen JC, Tan I-C, Aldrich MB, Adams KE, Wang X, et al. Near-infrared fluorescence imaging in humans with indocyanine green: A review and update. *The Open Surgical Oncology Journal*. 2020;**2**:12-25. DOI: 10.2174/1876504101002010012
- [28] Otani H, Engelman RM, Breyer RH, Rousou JA, Lemeshow S, Das DK. Mepacrine, a phospholipase inhibitor. A potential tool for modifying myocardial reperfusion injury. *Journal*

- of Thoracic and Cardiovascular Surgery. 1986;**92**:247-254. DOI: 10.1016/S0022-5223(19)35905-7
- [29] van Bilsen M, van der Vusse GJ, Willemsen PHM, Coumans WA, Roemen THM, Reneman RS. Effects of nicotinic acid and mepacrine on fatty acid accumulation and myocardial damage during ischemia and reperfusion. *Journal of Molecular and Cellular Cardiology*. 1990;**22**:155-163. DOI: 10.1016/0022-2828(90)91112-K
- [30] Canham LT. Silicon quantum wire array fabrication by electrochemical and chemical dissolution of wafers. *Applied Physics Letters*. 1990;**57**:1046-1048. DOI: 10.1063/1.103561
- [31] Heinrich JL, Curtis CL, CREDO GM, Sailor MJ, Kavanagh KL. Luminescent colloidal silicon suspensions from porous silicon. *Science*. 1992;**255**:66-68. DOI: 10.1126/science.255.5040.66
- [32] Wilson WL, Szajowski PF, Brus LE. Quantum confinement in size-selected, surface-oxidized silicon nanocrystals. *Science*. 1993;**262**:1242-1244. DOI: 10.1126/science.262.5137.1242
- [33] Mangolini L, Kortshagen U. Plasma-assisted synthesis of silicon nanocrystal inks. *Advanced Materials*. 2007;**19**:2513-2519. DOI: 10.1002/adma.200700595
- [34] Wang L, Reipa V, Blasic J. Silicon nanoparticles as a luminescent label to DNA. *Bioconjugate Chemistry*. 2004;**15**:409-412. DOI: 10.1021/bc030047k
- [35] Li ZF, Ruckenstein E. Water-soluble poly(acrylic acid) grafted luminescent silicon nanoparticles and their use as fluorescent biological staining labels. *Nano Letters*. 2004;**4**:1463-1467. DOI: 10.1021/nl0492436
- [36] Bayliss SC, Heald R, Fletcher DI, Buckberry LD. The culture of mammalian cells on nanostructured silicon. *Advanced Materials*. 1999;**11**:318-321. DOI: 10.1002/(SICI)1521-4095(199903)11:4<318::AID-ADMA318>3.0.CO;2-Z
- [37] Canham LT. Bioactive silicon structure fabrication through nanoetching techniques. *Advanced Materials*. 1995;**7**:1033-1037. DOI: 10.1002/adma.19950071215
- [38] Cunin F, Schmedake TA, Link JR, Li YY, Kom J, Bhatia SN, et al. Biomolecular screening with encoded porous-silicon photonic crystals. *Nature Materials*. 2002;**1**:39-41. DOI: 10.1038/nmat702
- [39] Salonen J, Kaukonen AM, Hirvonen J, Lehto VP. Mesoporous silicon in drug delivery applications. *Journal of Pharmaceutical Sciences*. 2008;**97**:632-653. DOI: 10.1002/jps.20999
- [40] Popplewell JF, King SJ, Day JP, Ackrill P, Fifield LK, Cresswell RG, et al. Kinetics of uptake and elimination of silicic acid by a human subject: A novel application of ³²Si and accelerator mass spectrometry. *Journal of Inorganic Biochemistry*. 1998;**69**:177-180. DOI: 10.1016/S0162-0134(97)10016-2
- [41] Galagudza M, Korolev D, Postnov V, Naumisheva E, Grigorova Y, Uskov I, et al. Passive targeting of ischemic-reperfused myocardium with adenosine-loaded silica nanoparticles. *International Journal of Nanomedicine*. 2012;**7**:1671-1678. DOI: 10.2147/IJN.S29511
- [42] Kalash RS, Lakshmanan VK, Cho CS, Park IK. *Theranostics. Biomaterials Nanoarchitectonics*. William Andrew Publishing; 2016:197-215. DOI: 10.1016/B978-0-323-37127-8.00012-1

- [43] De Salamanca AE, Diebold Y, Calonge M, García-Vazquez C, Callejo S, Vila A, et al. Chitosan nanoparticles as a potential drug delivery system for the ocular surface: Toxicity, uptake mechanism and in vivo tolerance. *Investigative Ophthalmology and Visual Science*. 2006;**47**:1416-1425. DOI: 10.1167/iovs.05-0495
- [44] Li L, Chen D, Zhang Y, Deng Z, Ren X, Meng X, et al. Magnetic and fluorescent multifunctional chitosan nanoparticles as a smart drug delivery system. *Nanotechnology*. 2007;**8**:405102. DOI: 10.1088/0957-4484/18/40/405102
- [45] Prabakaran M. Chitosan-based nanoparticles for tumor-targeted drug delivery. *International Journal of Biological Macromolecules*. 2015;**72**:1313-1322. DOI: 10.1016/j.ijbiomac.2014.10.052
- [46] Lila ASA, Ishida T, Allen TM. Liposomal nanomedicines. In: Torchilin V, editor. *Handbook of Nanobiomedical Research: Fundamentals, Applications, and Recent Developments*. Vol. 3. New Jersey: World Scientific; 2014. pp. 1-53. DOI: 10.1142/9789814520652_0001
- [47] Li P, Dai YN, Zhang JP, Wang AQ, Wei Q. Chitosan-alginate nanoparticles as a novel drug delivery system for nifedipine. *International Journal of Biomedical Sciences*. 2008;**4**:221-228
- [48] Istomina MS, Korolev DV, Pochkaeva EI, Mazing DS, Moshnikov VA, Gareev KG, et al. Study of the possibility of using of colloidal quantum dots based on AgInS₂/ZnS for fluorescence imaging in comparison with fluorophores fixed on the surface of the nanoparticles. *Translational Medicine*. 2017;**4**:56-65. DOI: 10.18705/2311-4495-2017-4-4-56-65
- [49] Istomina MS, Pochkaeva EI, Sonin DL, Pechnikova NA, Postnov VN, Mazing DS, et al. Research of the peculiarities of colloidal quantum dots of AgInS₂/ZnS and chitosan nanoparticles labeled with indocyanine green as the fluorescent labels for biomedical applications. *Regional Blood Circulation and Microcirculation*. 2018;**17**:74-82. DOI: 10.24884/1682-6655-2018-17-1-74-82
- [50] Korolev DV, Shulmeister GA, Romanova TN, Postnov VN. Investigation of the effectiveness of various organic solvents in the synthesis of aminospacer on magnetic nanoparticles. *Biotech*. 2018;**2**:40-44
- [51] Belorus AO, Beshpalova K, Spivak YM. Morphology and internal structure of porous silicon powders in dependence on the conditions of post-processing. In: *Proceedings of the 2016 IEEE North West Russia Section Young Researchers in Electrical and Electronic Engineering Conference (EIConRusNW 2016)*. Institute of Electrical and Electronics Engineers, Inc.; 2016. pp. 23-28. DOI: 10.1109/EIConRusNW.2016.7448108
- [52] Spivak YM, Belorus AO, Somov PA, Tulenin SS, Beshpalova KA, Moshnikov VA. Porous silicon nanoparticles for target drug delivery: Structure and morphology. *Journal of Physics: Conference Series*. 2015;**643**:12022. DOI: 10.1088/1742-6596/643/1/012022
- [53] Spivak YM, Belorus AO, Panevin AA, Zhuravskii SG, Moshnikov VA, Beshpalova K, et al. Porous silicon as a nanomaterial for disperse transport systems of targeted drug delivery to the inner ear. *Technical Physics*. 2018;**63**:1352-1360. DOI: 10.1134/S1063784218090207
- [54] Sonin D, Pochkaeva E, Zhuravskii S, Postnov V, Korolev D, Vasina L, et al. Biological safety and biodistribution of chitosan nanoparticles. *Nanomaterials*. 2020;**10**:810. DOI: 10.3390/nano10040810

[55] Wei Y, Zhao L. Passive lung-targeted drug delivery systems via intravenous administration. *Pharmaceutical Development and Technology*. 2014;**19**:129-136. DOI: 10.3109/10837450.2012.757782

[56] Abra RM, Hunt CA, Lau DT. Liposome disposition in vivo vi: Delivery to the lung. *Journal of Pharmaceutical Sciences*. 1984;**73**: 203-206. DOI: 10.1002/jps.2600730214

[57] Croce AC, Bottiroli G. Autofluorescence spectroscopy and imaging: A tool for biomedical research and diagnosis. *European Journal of Histochemistry*. 2014;**58**:320-337. DOI: 10.4081/ejh.2014.2461

[58] Whittington NC, Wray S. Suppression of red blood cell autofluorescence for immunocytochemistry on fixed embryonic mouse tissue. *Current Protocols in Neuroscience*. 2017;**81**:2.28.1-2.28.12. DOI: 10.1002/cpns.35

[59] Lerchenberger M, Al Arabi N, Gallwas JKS, Stepp H, Hallfeldt KKJ, Ladurner R. Intraoperative near-infrared autofluorescence and indocyanine green imaging to identify parathyroid glands: A comparison. *International Journal of Endocrinology*. 2019;**2019**:1-7. DOI: 10.1155/2019/4687951

[60] Smith AM, Mancini MC, Nie S. Bioimaging: Second window for in vivo imaging. *Nature Nanotechnology*. 2009;**4**:710-711. DOI: 10.1038/nnano.2009.326

[61] Inyushin M, Meshalkina D, Zueva L, Zayas-Santiago A. Tissue transparency in vivo. *Molecules*. 2019;**24**:1460. DOI: 10.3390/molecules24132388